Analytical beam propagation model for clipped focused-Gaussian beams using vector diffraction theory

Glen D. Gillen[1], Christopher M. Seck[1*], and Shekhar Guha[2]

[1]*Physics Department, California Polytechnic State University, San Luis Obispo, CA, 93407, USA*
[2]*Air Force Research Laboratory, Materials and Manufacturing Directorate, Wright-Patterson Air Force Base, Dayton, OH, 45433,USA*
[*]*Current address: Physics Department, Northwestern University, Evanston, IL, 60208, USA*
ggillen@calpoly.edu

Abstract: Vector diffraction theory is applied to the case of focused TEM_{00} Gaussian beams passing through a spatially limiting aperture in order to investigate the propagation of these clipped focused-Gaussian beams. Beam distributions at different axial distances show that a traditional M^2 propagation model cannot be used for the propagation of clipped focus-Gaussian beams. Using Luneberg's vector diffraction theory and Fresnel approximations, an analytical model for the on-axis transverse and longitudinal electric fields and intensity distributions is presented including predictions of the maximum obtainable intensity. In addition, an analytical expression is provided for the longitudinal component of the electric field of a TEM_{00} mode unperturbed Gaussian beam. Experimental results are also presented and compared to the model's predictions.

OCIS codes: (050.1220) apertures; (050.1960) Diffraction theory; (220.2560) propagating methods

References and links

1. H. Kogelnik and T. Li, "Laser beam resonators," Proc. IEEE **54**, 1312–1329 (1966).
2. A. Yariv, *Quantum Electronics*, Third Edition, (John Wiley & Sons, New York, NY, 1989.)
3. W. T. Sifvast, *Laser Fundamentals*, (Cambridge University Press, New York, NY, 1996.)
4. A. E. Siegman, *Lasers*, (University Science Books, Mill Valley, CA, 1986.)
5. M. W. Sasnett, *Physics and Technology of Laser Resonators*, (Hilger, New York, NY 1989.)
6. A. E. Siegman, "New Developments in Laser Resonators," Proc. SPIE **1224**, 2–12 (1990).
7. I. Ghebregziabher and B. C. Walker, "Effect of focal geometry on radiation from atomic ionization in an ultra-strong and ultrafast laser field," Phys. Rev. A **76**, 023415 (2007).
8. J. M. P. Coelho, M. A. Abreu, and F. C. Rodrigues, "Modelling the spot shape influence on high-speed transmission lap welding of thermoplastic films," J. Opt. Lasers Eng. **46**, 55–61 (2007).
9. Y. Li, "Focal shifts in diffracted converging electromagnetic waves. I. Kirchhoff theory," J. Opt. Soc. Am. A **22**, 68–76 (2005).
10. Y. Li, "Focal shifts in diffracted converging electromagnetic waves. II. Rayleigh theory," J. Opt. Soc. Am. A **22**, 77–83 (2005).
11. G. P. Agrawal and D. N. Pattanayak, "Gaussian beam propagation beyond the paraxial approximation," J. Opt. Soc. Am. **69**, 575–578 (1979).
12. C. G. Chen, P. T. Konkola, J. Ferrera, R. K. Heilmann, and M. L. Schattenburg, "Analyses of vector Gaussian beam propagation and the validity of paraxial and spherical approximations," J. Opt. Soc. Am. A **19**, 404–412 (2002).

#121792 - $15.00 USD Received 21 Dec 2009; revised 7 Feb 2010; accepted 9 Feb 2010; published 16 Feb 2010

13. B. Lü and K. Duan, "Nonparaxial propagation of vectorial Gaussian beams diffracted at a circular aperture," Opt. Lett. **28**, 2440–2442 (2003).
14. K. Duan and B. Lü, "Vectorial nonparaxial propagation equation of elliptical Gaussian beams in the presence of a rectangular aperture," J. Opt. Soc. Am. A **21**, 1613–1620 (2004).
15. K. Duan and B. Lü, "Polarization properties of vectorial nonparaxial Gaussian beams in the far field," Opt. Lett. **2005**, 308–310 (2005).
16. G. Bekefi, "Diffraction of electromagnetic waves by an aperture in a large screen," J. Appl. Phys. **24**, 1123–1130 (1953).
17. S. Guha and G. D. Gillen, "Description of light propagation through a circular aperture using nonparaxial vector diffraction theory," Opt. Express **13**, 1424–1447 (2005).
18. G. D. Gillen, K. Baughman, and S. Guha, "Application of Hertz vector diffraction theory to the diffraction of focused Gaussian beams and calculations of focal parameters," Opt. Express **17,** 1478–1492 (2009).
19. W. H. Carter, "Electromagnetic field of a Gaussian beam with an elliptical cross section," J. Opt. Soc. Am. **62**, 1195–1201 (1972).
20. M. Lax, W. H. Louisell and W. B. McKnight, "From Maxwell to paraxial wave optics," Phys. Rev. A **11**, 1365–1370 (1975).
21. L. Cicchitelli, H. Hora and R. Postle, "Longitudinal field components for laser beams in vacuum," Phys. Rev. A **41**, 3727–3732 (1990).
22. M. O. Scully, "A simple laser linac," Appl. Phys. B **51**, 238–241 (1990).
23. J. J. Macklin, J. K. Trautman, T. D. Harris and L. E. Brus, "Imaging and time-resolved spectroscopy of single molecules at an interface," Science **272**, 255–258 (1996).
24. L. Novotny, M. R. Beversluis, K. S. Youngworth and T. G. Brown, "Longitudinal field modes probed by single molecules," Phys. Rev. Lett. **86**, 5251–5254 (2001).
25. S. Takeuchi, R. Sugihara and K. Shimoda, "Electron acceleration by longitudinal electric field of a Gaussian laser beam," J. Phys. Soc. Jpn. **63**, 1186-1193 (1994).
26. J. P. Paquette and J. L. Chaloupka, "Effect of realistic focal conditions on the strong-field ionization of helium," Phys. Rev. A **79**, 043410 (2009).
27. G. D. Gillen and S. Guha, "Modeling and propagation of near-field diffraction patterns: a more complete approach," Am. J. Phys. **72**, 1195–1201 (2004).
28. R. K. Luneberg, *Mathematical theory of optics*, (University of California Press, Berkeley, California, 1964.)
29. A. J. Campillo, J. E. Pearson, S. L. Shapiro, and N. J. Terrell, Jr., "Fresnel diffraction effects in the design of high-power laser systems," Appl. Phys. Lett. **23**, 85–87 (1973).

1. Introduction

Due to the physical characteristics of many laser cavities, the output of a large percentage of commercial laser systems is either a pure Gaussian or a lower mode Hermite-Gaussian beam. Predicting and understanding the behavior and propagation of pure (TEM_{00}) Gaussian beams can be best described by the mathematical model presented by Kogelnik and Li [1], and later in Yariv's text [2]. If the light beam is predominantly Gaussian, but contains higher order Hermite-Gaussian modes, is only partially coherent, or is imperfect for other reasons, the M^2 beam propagation model [3] is commonly used. The origin of the M^2 model comes from Siegman's book [4] where he describes an aperture at the beam waist of a focused laser beam, and the aperture is at least a few times larger than the beam waist. For this configuration, the number of Hermite-Gaussian modes which will 'fit' inside of the aperture is N, and the product of the beam waist and the divergence angle results in a factor of N^2. A few years later, Siegman's model was applied and adapted to describe the beam quality, propagation and focusability of not just multi-mode beams, but also incoherent and other non-diffraction-limited beams [5, 6]. Since its introduction, M^2 beam propagation models have been used by laser manufacturers to characterize the overall Gaussian quality of the output beams, and to predict the focal behavior of the focused beam; i.e., focal spot size, peak obtainable intensity ('intensity' used here synonymously with irradiance), and convergence angle.

Theoretically, TEM_{00} Gaussian beams extend out radially to infinity. Experimentally, optical components and other experimental apparati have limited sizes. When dealing with laser beams in laboratory settings, there has always been a trade off between size limitations of the beams being used and size limitations of the physical components. All experimental beams are clipped

#121792 - $15.00 USD Received 21 Dec 2009; revised 7 Feb 2010; accepted 9 Feb 2010; published 16 Feb 2010

to some degree by the edges of lenses, mirrors, apertures, entrance windows to vacuum chambers, dewars, etc. Many fields of study in science and engineering from atomic physics [7] to industrial laser welding [8] are concerned with accurate knowledge of focal intensity distributions *and* maximizing peak focal intensities. Given a fixed optical component, higher peak intensities can be achieved by enlarging the beam width incident upon the focusing optic at the expense of clipping off more and more of the wings of the Gaussian beam. To the best of the authors' knowledge an analytical model does not exist for predicting the effects of clipping on the peak obtainable intensities based upon the clipping ratio between the beam size and the size of the limiting aperture.

Diffraction theory models of beam propagation are used when the electromagnetic fields are known across a specific surface before the point of interest, and when the electromagnetic fields at a specific point of interest are desired. The input plane is typically a transmission limiting aperture where propagation of light through the input surface is spatially limited to a particular area and the rest of the surface is opaque. Beyond plane-wave input light fields, non-paraxial diffraction theory has been applied to converging spherical waves [9, 10], and diverging Gaussian beam [11–15] light fields. One limitation of the models presented in Refs. [11–15] is that the aperture plane is chosen to be coplanar with the beam waist of the Gaussian light field. Recently, we applied Hertz vector diffraction theory (HVDT) [16, 17] to the diffraction of converging focused Gaussian light fields (GHVDT) [18] and investigated the effects of diffraction on the behavior and propagation of the electromagnetic fields. In Ref. [18] it was shown that GHVDT can serve as a single mathematical model which can reproduce results from the purely Gaussian regime (Refs. [1, 2]) when the aperture is much larger than the beam to the purely diffractive regime (Ref. [17]) when the aperture is much smaller than the beam, and any regime in between.

In this paper we first apply GHVDT to the diffraction of clipped focused-Gaussian laser beams. The GHVDT beam propagation model is used to calculate radial intensity distributions over a range of axial distances in the vicinity of the focal region. The M^2 beam width versus axial distance model is applied to the intensity distributions calculated using GHVDT to test the validity of the M^2 model to this particular form of non-diffraction-limited beams. It is shown that the M^2 model does not accurately predict correct beam widths and their asymmetrical behavior as a function of axial position.

The longitudinal component of the electric field of a Gaussian beam is derived automatically when GHVDT is used. Several authors have addressed the analysis of the longitudinal component of the focused light beams. Carter showed that a focused light beam has a longitudinal component [19]. Lax, Louisell and McKnight showed a way to calculate the longitudinal component under the paraxial approximation using a perturbation analysis [20]. The longitudinal component needed to be included in the analysis for the fields to satisfy Maxwells equations. Cicchitelli, Hora and Postle extended the analysis to the non-paraxial case, i.e., tighter focusing [21]. Several applications using the longitudinal component of the electric field were proposed, including acceleration of charged particles to high energies [22] and probing of the absorption dipole moments of single molecules [23, 24]. Analytical expression for the longitudinal electric field component of the (1,0) mode of a Hermite Gaussian beam was presented by Scully [22] and Takeuchi *et al.* [25]. Paquette and Chaloupka recently studied the effects of the longitudinal electric field component on the double ionization of helium by tightly focused high intensity laser beam [26]. Here we derive the expression for the longitudinal component of the electric field for the TEM_{00} mode of a paraxial Gaussian beam using Luneberg's vector diffraction theory and obtain an expression identical with that derived by Lax *et al.*

Although GHVDT is mathematically complete and produces accurate results for modeling the propagation of clipped focused-Gaussian beams for all locations within and beyond the

#121792 - $15.00 USD Received 21 Dec 2009; revised 7 Feb 2010; accepted 9 Feb 2010; published 16 Feb 2010

aperture, it does have two drawbacks: (1) to calculate high-resolution field and intensity distributions it can become quite computationally time-intensive, and (2) due to its complicated differential and integral mathematics analytical solutions are not easily obtained. Here we will show that for points where the axial distance is larger than the aperture radius a simpler vector diffraction theory can be used to: (1) obtain integral solutions for the transverse and the longitudinal components of the electric field which are computationally faster than GHVDT, and (2) obtain analytical solutions to calculate the vector components of the electric field for on-axis locations. Using Luneberg's vector diffraction theory, general nonparaxial expressions for the three components of the electric field are obtained in terms of double integrals. Under Fresnel approximations, these integral expressions are much simplified and the transverse electric field component reduces to the common expression derived under scalar Huygens-Fresnel theory. For two special cases of unclipped beam and on-axis distributions, the integrals can be analytically evaluated. The analytical model is used to calculate on-axis intensities for a variety of clipping ratios. Predicted on-axis intensities and their asymmetrical behavior are presented along with experimental verification for the first time. The final goal of this paper is to present a simple analytical model which can be used to quickly determine peak obtainable focal intensities for clipped beams as a function of the clipping ratio with experimental verification.

2. Luneberg's Vector Diffraction Theory

Beginning with Green's scalar theorem for any two scalar functions, U and V,

$$\iint_S \left(U\vec{\nabla}V - V\vec{\nabla}U\right)\cdot\hat{n}\,ds = \iiint_v \left(U\nabla^2 V - V\nabla^2 U\right)\,dv, \tag{1}$$

the diffraction integrals for scalar diffraction theory can be derived [27]. If the region of space of interest is restricted to be free of charges, the diffracting aperture plane is that of surface S_o, V is chosen to be the scalar electric field of the incident light, and U is chosen to be a Green's function then Eq. 1 can be expressed as [28]

$$E\left(\vec{r}\right) = -\frac{1}{2\pi}\iint_{S_o} E\left(\vec{r_o}\right)\left(\frac{\partial G}{\partial z}\right)_{S_o} ds_o \tag{2}$$

where G is the Green's function,

$$G = \frac{e^{-ik\rho}}{\rho} \tag{3}$$

and ρ is the distance from a point in the aperture plane, (x_o, y_o, z_o), to the point of interest, (x, y, z), or

$$\rho^2 = |\vec{r} - \vec{r_o}|^2 = (x - x_o)^2 + (y - y_o)^2 + (z - z_o)^2\,. \tag{4}$$

The partial derivative with respect to the axial location of the point of interest, z, of Eq. 2 is

$$\frac{\partial G}{\partial z} = -ikz\left(1 + \frac{1}{ik\rho}\right)\frac{e^{-ik\rho}}{\rho^2}. \tag{5}$$

Scalar diffraction theories derived from Green's theorem generally choose the light field within the aperture plane, $E\left(\vec{r_o}\right)$, to be the same as that of the incident light field. For this paper, it is chosen that the incident light field is that of a focused TEM_{00} Gaussian beam with an electric field represented as [2]

$$E\left(x_o, y_o, z_o\right) = \frac{E_o}{\left(1 + \frac{z_o - z_G}{q_o}\right)} e^{-\frac{ik\left(x_o^2 + y_o^2\right)}{2\left(q_o + z_o - z_G\right)} - ik\left(z_o - z_G\right)} \tag{6}$$

#121792 - $15.00 USD Received 21 Dec 2009; revised 7 Feb 2010; accepted 9 Feb 2010; published 16 Feb 2010

where E_o is the incident field amplitude, z_G is the axial location of the focal plane, and q_o is the complex focal parameter

$$q_o = \frac{i\pi\omega_o^2 n}{\lambda} \tag{7}$$

with ω_o representing the e^{-1} half-width of the electric field, or the e^{-2} half-width of the intensity in the focal plane, n is the refractive index of the medium the beam is traveling through, and λ is the wavelength of the light field. The parameters z_G and ω_o are illustrated in Fig. 1, the theoretical setup used in this investigation, along with the additional parameters, ω_a and r_c representing the unperturbed beam width in the aperture plane and the clipping aperture radius, respectively.

If $z_G = z_o$ the focal plane is coplanar with the aperture plane; an assumption frequently used for other scalar and vector diffraction models for Gaussian beams [9–13]. Although this assumption greatly simplifies the mathematics for calculating fields for points beyond the aperture plane, it limits the use of these models to the diffraction of Gaussian beams where the diffraction plane can only occur at the location of the beam's minimum waist. Throughout this manuscript, z_G is retained as an independent parameter. In addition to the value of $z_o - z_G$ describing the axial location of the unperturbed focal plane, the sign of $z_o - z_G$ determines whether or not the incident Gaussian light field is converging or diverging. The rest of this manuscript will assume that $z_G - z_o$ has a positive value representing the diffraction of a converging focused-Gaussian light field. This particular choice for z_G is such that the diffraction effects of a clipped focused-Gaussian beam can be studied and the effects of diffraction on the focal behavior of the light fields can be quantified in order to present an analytical beam propagation model for clipped-Gaussian beams.

Substitution of Eqs. 5 and 6 into Eq. 2, and defining the location of the $z_o = 0$ plane to be

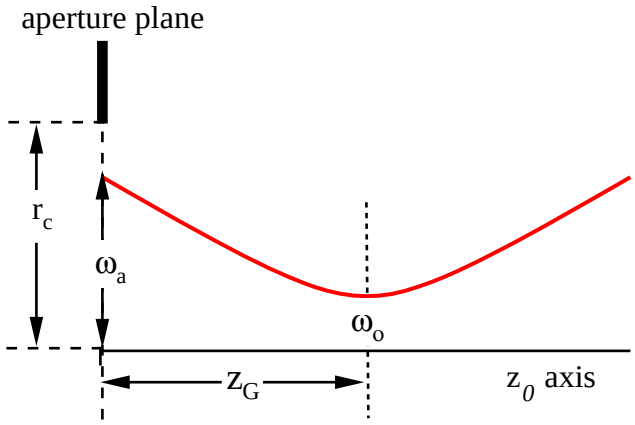

Fig. 1. Theoretical setup used in this investigation where ω_o is the unperturbed minimum beam half-width, ω_a is the unperturbed beam half-width in the aperture plane, r_c is the radius of the clipping aperture, and z_G is axial the distance from the aperture to the unperturbed beam waist.

#121792 - $15.00 USD Received 21 Dec 2009; revised 7 Feb 2010; accepted 9 Feb 2010; published 16 Feb 2010

that of the diffracting surface, we get

$$E_x(x,y,z) = \frac{ikzE_o e^{ikz_G}}{2\pi\left(1-\frac{z_G}{q_o}\right)} \iint e^{-\frac{ik\left(x_o^2+y_o^2\right)}{2(q_o-z_G)}} \frac{e^{-ik\rho}}{\rho^2}\left(1+\frac{1}{ik\rho}\right) dx_o dy_o \tag{8}$$

where it has been assumed that the incident light field is polarized in the x-dimension. The limits of the integral in Eq. 8 are the edges of the open area of the aperture.

Equation 8 has been obtained through scalar diffraction theory based upon Green's scalar theorem and is frequently referred to as the Rayleigh-Sommerfeld diffraction integral. Similarly, starting with Green's scalar theorem Luneberg developed a vector diffraction theory using the electromagnetic wave property that $\vec{\nabla}\cdot\vec{E}=0$ [28]. Using Luneberg's variation of vector diffraction theory, the x-component of the field at the point of interest is Eq. 2, and the y and z-components can be expressed as

$$E_y(\vec{r}) = -\frac{1}{2\pi}\iint_{S_o} E_y(\vec{r_o})\left(\frac{\partial G}{\partial z}\right)_{S_o} ds_o, \tag{9}$$

and

$$E_z(\vec{r}) = \frac{1}{2\pi}\iint_{S_o}\left[E_x(\vec{r_o})\left(\frac{\partial G}{\partial x}\right)_{S_o} + E_y(\vec{r_o})\left(\frac{\partial G}{\partial y}\right)_{S_o}\right] ds_o, \tag{10}$$

respectively (see Eq. 45.76 of ref. [28]). Following the same procedure as Eq. 8, and assuming that the incident light is polarized in the x-direction, the field components E_y and E_z become

$$E_y(x,y,z) = 0 \tag{11}$$

and

$$E_z(x,y,z) = \frac{ikE_o e^{ikz_G}}{2\pi\left(1-\frac{z_G}{q_o}\right)} \iint e^{-\frac{ik\left(x_o^2+y_o^2\right)}{2(q_o-z_G)}} \frac{e^{-ik\rho}}{\rho^2}\left(1+\frac{1}{ik\rho}\right)(x-x_o)\, dx_o dy_o. \tag{12}$$

Equations 8, 11, and 12 are the general integral results of this paper for the diffraction of focused Gaussian beams using Luneberg vector diffraction theory.

3. Analytical beam propagation model

One of the objectives of this paper is to develop an analytical beam propagation model for focused TEM_{00} Gaussian beams clipped by a circular aperture (or other spatial limitation on the radial size of the beam.) To simplify the mathematics two mathematical assumptions will be employed. It will first be assumed that $\rho \gg \lambda$. This assumption forces the parenthesis at the end of Eq. 8 to be 1. Using cylindrical coordinates, Eqs. 8 and 12 become

$$E_x(r,\theta,z) = \frac{ikzE_o e^{ikz_G}}{2\pi\left(1-\frac{z_G}{q_o}\right)} \iint e^{-\frac{ikr_o^2}{2(q_o-z_G)}} \frac{e^{-ik\rho}}{\rho^2} r_o dr_o d\theta_o, \tag{13}$$

and

$$E_z(r,\theta,z) = \frac{ikE_o e^{ikz_G}}{2\pi\left(1-\frac{z_G}{q_o}\right)} \iint e^{-\frac{ikr_o^2}{2(q_o-z_G)}} \frac{e^{-ik\rho}}{\rho^2}\left(r\cos\theta - r_o\cos\theta_o\right) r_o dr_o d\theta_o \tag{14}$$

The second assumption in this section will use the Fresnel approximation to simplify the integrals. Here it is assumed that $z > r_c$; i.e., the distance from the aperture plane to the axial distance of the point of interest is greater than the radius of the diffracting aperture. This

#121792 - $15.00 USD Received 21 Dec 2009; revised 7 Feb 2010; accepted 9 Feb 2010; published 16 Feb 2010

assumption corresponds to optical systems with f numbers of 0.5 or higher, which is true for most practical systems. Thus, ρ can be expanded as a Taylor series. For terms in Eq. 13 and 14 where ρ appears in the phase, the first two terms of the Taylor series expansion are retained. For terms where ρ appears in the amplitude, only the first term of the Taylor series expansion is used. Application of these assumptions and approximations to Eqs. 13 and 14 yield integral expressions for the x and z-components of the electric field as

$$E_x(r,\theta,z) = \frac{ikE_o e^{ik(z_G-z)} e^{-\frac{ikr^2}{2z}}}{z\left(1-\frac{z_G}{q_o}\right)} \int e^{-ik\left(\frac{1}{2(q_o-z_G)}+\frac{1}{2z}\right)r_o^2} J_0\left(\frac{krr_o}{z}\right) r_o dr_o. \tag{15}$$

and

$$E_z(r,\theta,z) = \frac{ikE_o\cos\theta e^{ik(z_G-z)} e^{-\frac{ikr^2}{2z}}}{z^2\left(1-\frac{z_G}{q_o}\right)} \int \quad e^{-ik\left(\frac{1}{2(q_o-z_G)}+\frac{1}{2z}\right)r_o^2} \times \left[rJ_0\left(\frac{krr_o}{z}\right) - ir_o J_1\left(\frac{krr_o}{z}\right)\right] r_o dr_o. \tag{16}$$

Equations 15 and 16 constitute the Fresnel approximations of the general integral solutions, Eqs. 8 and 12, of the model presented in this manuscript.

For integration purposes, Eqs. 15 and 16 can be more conveniently expressed as

$$E_x(r,\theta,z) = Ae^{-\frac{ikr^2}{2z}} \int e^{-ar_o^2} J_0(\beta r_o)\, r_o dr_o \tag{17}$$

and

$$E_z(r,\theta,z) = Ae^{-\frac{ikr^2}{2z}} \frac{\cos\theta}{z} \int e^{-ar_o^2} \left[rJ_0(\beta r_o) - ir_o J_1(\beta r_o)\right] r_o dr_o, \tag{18}$$

where

$$A = \frac{ikE_o e^{ik(z_G-z)}}{z\left(1-\frac{z_G}{q_o}\right)}, \tag{19}$$

$$a = ik\left(\frac{1}{2(q_o-z_G)}+\frac{1}{2z}\right) \text{ , and } \beta = \frac{kr}{z}. \tag{20}$$

For unperturbed focused Gaussian beam propagation, the upper limit of the radial integral goes to infinity, and analytical solutions to Eqs. 17 and 18 can be found to be

$$E_x(r,\theta,z) = \frac{E_o}{\left(1+\frac{z-z_G}{q_o}\right)} e^{-\frac{ikr^2}{2(q_o+z-z_G)}-ik(z-z_G)} \tag{21}$$

and

$$E_z(r,\theta,z) = \frac{E_o r\cos\theta}{q_o\left(1+\frac{z-z_G}{q_o}\right)^2} e^{-\frac{ikr^2}{2(q_o+z-z_G)}-ik(z-z_G)} \tag{22}$$

or

$$E_z(r,\theta,z) = E_x(r,\theta,z)\frac{r\cos\theta}{(q_o+z-z_G)}. \tag{23}$$

Note that after using paraxial approximations and integration, the x-component of the model presented here yields the exact expression as Eq. 6 (the scalar beam propagation model of

#121792 - $15.00 USD Received 21 Dec 2009; revised 7 Feb 2010; accepted 9 Feb 2010; published 16 Feb 2010

Refs. [1, 2]) for an unperturbed focused Gaussian beam. To the best of the authors' knowledge, the analytical expression presented in Eq. 23 for the longitudinal component of the electric field for focused Gaussian beams does not currently exist in the literature.

Equation 23 allows a rough estimation of the magnitude of the longitudinal field component with respect to the dominant transverse component E_x by normalizing E_z to E_x, or

$$\frac{E_z(x,y,z)}{E_x(x,y,z)} = \frac{x}{(q_o + z - z_G)}. \tag{24}$$

In the focal plane, $z = z_G$, the ratio of the longitudinal to the transverse field components becomes

$$\frac{E_z}{E_x} = -\frac{ix}{z_R}. \tag{25}$$

where the term z_R is the Rayleigh range [2], and is related to the complex focal parameter q_o by $q_o = iz_R$ or

$$z_R = \frac{\pi \omega_o^2 n}{\lambda}. \tag{26}$$

The maximum value of E_z in the focal plane occurs when $x = \frac{\omega_o}{\sqrt{2}}$, and the ratio of the longitudinal component to the transverse component becomes

$$\left(\frac{E_z}{E_x}\right)_{max} = \frac{-i\lambda}{\pi\sqrt{2}\omega_o}. \tag{27}$$

For a very tightly focused beam such that $\omega_o \approx \lambda$, this ratio becomes $\sim \frac{-i}{\pi\sqrt{2}}$; i.e., the peak intensity of the longitudinal component can be upwards of 5 % of the transverse component. The effects of the longitudinal component in nonlinear optical experiments with tight focusing may be non-negligible.

The intensity, or modulus square, of each field component can be found to be

$$|E_x|^2 = \frac{E_o^2}{1 + \frac{(z - z_G)^2}{Z_R^2}} e^{-2\frac{r^2}{\omega^2(z)}}, \tag{28}$$

and

$$|E_z|^2 = |E_x|^2 \frac{r^2 \cos^2\theta}{z_R^2 \left(1 + \frac{(z - z_G)^2}{z_R^2}\right)}. \tag{29}$$

For clipped focused Gaussian beams the x and z-components of the field are determined by Eqs. 17 and 18 where the upper limit of the integral is the radius of the clipping aperture, r_c. In order to obtain a simplified analytical model, it will now be assumed that the points of interest beyond the aperture plane reside along the axis of propagation, or $r = x = y = 0$. For on-axis locations, the x-component of the field becomes

$$E_x(0,\theta,z) = A \int_0^{r_c} e^{-ar_o^2} r_o dr_o. \tag{30}$$

By definition of Eq. 11, the y-component of the electric field is $E_y = 0$. Substitution of $r = 0$ into the integral for the z-component of the electric field, Eq. 18, is also zero for all on-axis positions, or

$$E_z(0,\theta,z) = 0. \tag{31}$$

#121792 - $15.00 USD Received 21 Dec 2009; revised 7 Feb 2010; accepted 9 Feb 2010; published 16 Feb 2010

With a straight-forward integration by parts, the complex electric field of Eq. 30 can be analytically represented as

$$E_x(z) = E_G(z)\left[1 - e^{-ar_c^2}\right]. \tag{32}$$

where

$$E_G(z) = \frac{A}{2a} = \frac{E_o}{1 + \frac{z - z_G}{q_o}} e^{-ik(z - z_G)} \tag{33}$$

is the function for the on-axis field of an unperturbed focused Gaussian beam.

Computing the modulus square of Eq. 32 and simplifying, the analytical on-axis intensity for a clipped focused Gaussian beam can be expressed as

$$I(z) = I_G(z)\left[1 + e^{-2\gamma^2} - 2e^{-\gamma^2}\cos\left(\frac{kr_c^2}{2}\left[\frac{1}{R_a} - \frac{1}{z}\right]\right)\right] \tag{34}$$

where

$$I_G(z) = \frac{E_o^2}{1 + \frac{(z - z_G)^2}{z_R^2}} \tag{35}$$

is the exact expression for the on-axis intensity function for an unperturbed TEM_{00} Gaussian beam. The variables γ and R_a in Eq. 34 are the clipping ratio and the radius of curvature of the wavefront at the focal plane, respectively. The radius of curvature of the wave front at the focal plane is

$$R_a = z_G\left(1 + \frac{z_R^2}{z_G^2}\right). \tag{36}$$

The clipping ratio is an important parameter in the propagation of diffracted focused Gaussian beams, and is the ratio of the aperture radius to the e^{-1} half-width of the electric field of the incident beam at the aperture plane, ω_a, or

$$\gamma = \frac{r_c}{\omega_a} \text{ where } \omega_a^2 = \omega_o^2\left(1 + \frac{z_G^2}{z_R^2}\right). \tag{37}$$

Equations 32 and 34 are expressed in the form where the on-axis electric field and intensity functions of a clipped Gaussian beam are equal to the unperturbed field and intensity functions multiplied by diffraction-dependent functions. Equations 32 and 34 constitute the general analytical solutions for this paper. Equation 34 represents an analytical model for the on-axis behavior of clipped focused-Gaussian beams as a function of the axial distance from the aperture plane.

A simpler version of Eq. 34 can be obtained if we restrict ourselves to on-axis locations near the focal plane, $z \approx z_G$, and restrict the aperture plane to be far from the focal plane with respect to the Rayleigh range, i.e., $z \gg z_R$ such that $R_a \approx z_G$. Thus, the maximum obtainable field intensity is just a function of the clipping ratio, or

$$I_{max}(\gamma)_{z \approx z_G} = I_{G_{max}}\left[1 + e^{-2\gamma^2} - 2e^{-\gamma^2}\right]. \tag{38}$$

Equation 38 represents a simple analytical model which can be used to quickly determine the maximum theoretical intensity in the focal plane for a clipped focused-Gaussian beam. The limitations of using Eq. 38 are discussed further in the next section.

#121792 - $15.00 USD Received 21 Dec 2009; revised 7 Feb 2010; accepted 9 Feb 2010; published 16 Feb 2010

4. Calculations and Experimental Verification

Using the previously established GHVDT model of full wave equation vector diffraction of clipped focused-Gaussian beams [18], radial intensity distributions are calculated for a variety of axial distances from the aperture plane, and for a variety of clipping ratio values. Calculated radial intensity distributions are then analyzed using a Gaussian fitting routine to obtain representative beam widths. For each clipping ratio value, the beam width versus axial distance data is then compared to the M^2 beam propagation model. The M^2 propagation model used is that described in section 11.3 of Ref. [3]. Figure 2 illustrates a collection of e^{-2} beam half-widths versus on-axis location graphs and their corresponding M^2 fits for clipping ratios of 3, 2, 1.5, and 1. The parameters chosen for Fig. 2 calculations are a wavelength of $\lambda = 780$ nm, a minimum beam waist of $\omega_o = 5\ \mu$m and an aperture to focal plane distance of $z_G = 99\ z_R = 1$ cm. Identical results are obtained if Eq. 8 is used instead of GHVDT. As illustrated in Fig. 2, for clipping ratios less than $\sim$2, the M^2 model begins to significantly deviate from calculated beam propagation behavior, and is thus not a valid model when describing the propagation of clipped focused-Gaussian beams. For reference, clipping ratios of 2, 1.5, and 1 correspond to only 0.5%, 3.4%, and 15.7% of the energy being blocked by the aperture, respectively. As the clipping ratio decreases for values less than 2, the effects of diffraction on the beam manifest themselves as an elongation of the focal region with larger and larger minimum beam waists. Having a longer collimated region can be useful in nonlinear optical frequency conversion or in measurement of third order optical nonlinearities. For clipping ratios of $\lesssim$1 the on-axis beam width behavior demonstrates asymmetric behavior away from the focal region as diffraction effects become a dominant influence upon beam propagation.

Figure 3 investigates the effects of clipping on the beam intensity distributions in the focal plane for an unperturbed focused Gaussian beam, $\gamma = 3$, and a clipped focused Gaussian beam, $\gamma = 1$. Figures 3(a) and (c) are two-dimensional images of the modulus square of the *x*-component of the electric field calculated using Eq. 17, and the modulus square of the *z*-component of the electric field calculated using Eq. 18, respectively. The parameters used for the calculations of Fig. 3 are the same as those used for Fig. 2(a) and (d), or $\omega_o = 5\mu$m, $z_G = 10$ mm, and $\lambda = 780$ nm. The color scales of both $|E_x|^2$ distributions are normalized to the peak value of $|E_x|^2$ for the unperturbed beam. Similarly, the color scales of both $|E_z|^2$ distributions are normalized to the peak value of $|E_z|^2$ for the unperturbed beam. As the clipping ratio decreases, the peak values of the intensity profiles decrease, and the overall width of both components of the electric field increases. Notice that the peak values for the clipped beam do not decrease equally for $|E_x|^2$ and $|E_z|^2$. The peak value of part (c) is 40 % of that of part (a), whereas the peak value of part (d) is only 21.7% of that of part (b). Similar intensity fluctuations for clipped Gaussian beams were investigated and observed by Campillo *et al.* [29].

Figure 4 investigates the effects of clipping on the beam intensity distributions for an off-focal plane axial location. The parameters used for the calculations of Fig. 4 are the same as those used for Figs. 2(d) and 3(c) & (d), or $\gamma = 1$, $\omega_o = 5\mu$m, $z_G = 10$ mm, and $\lambda = 780$ nm. Part (a) is a calculation of the on-axis intensity of the beam. Due to diffraction of the beam, the on-axis intensity distribution is no longer pure Lorentzian as it is for an unperturbed focused Gaussian beam. Away from the focal plane, oscillations are observed in the on-axis intensity distribution of part (a). Calculations performed for parts (b)–(d) are for the axial location of the on-axis minimum closest to the focal plane, or $z = 9.385$ mm, as indicated by the dashed line in part (a). Figure 4(b) is a radial beam distribution illustrating that the radial behavior of the beam is no longer Gaussian, and actually has a localized minimum in the middle of the beam, which is better observed in the two-dimensional beam profile of $|E_x|^2$ calculated in part (c). Part (d) is a calculation of the longitudinal component of the intensity, $|E_z|^2$. The effects of diffraction on the propagation behavior differences between focal plane and off-focal plane locations is

#121792 - $15.00 USD Received 21 Dec 2009; revised 7 Feb 2010; accepted 9 Feb 2010; published 16 Feb 2010

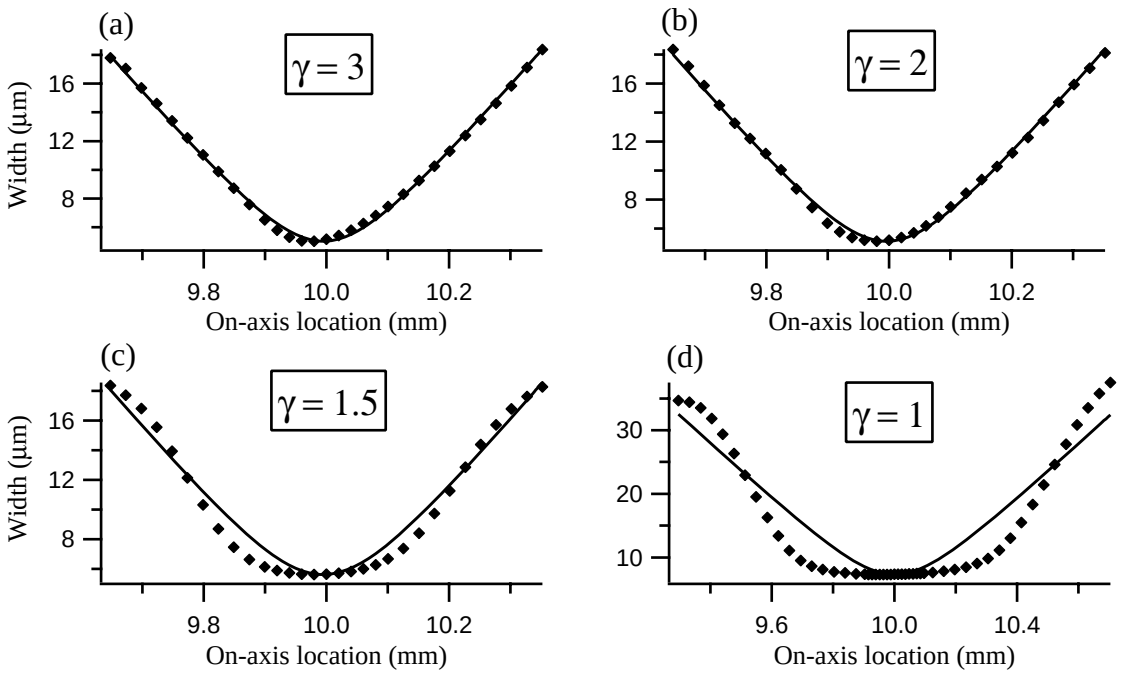

Fig. 2. Calculated e^{-2} beam half-widths of the intensity of a clipped focused-Gaussian beam using GHVDT (diamonds) and fits to the calculations using a traditional M^2 model (solid lines) for various clipping ratios, γ, between values of 3 and 1. All figures are for $\omega_o = 5\mu$m, $z_G = 10$ mm, and $\lambda = 780$ nm. The values of M^2 fit for each of the four cases are (a) 1.00, (b) 1.02,(c) 1.12, and (d) 1.32.

observed via the comparison of Figs. 3(c) & (d) and Figs. 4(c) & (d).

One of the main theoretical results of this manuscript is the analytical expression for the on-axis intensity, Eq. 34, and its simpler form, Eq. 38. Using Eqs. 34 and 38, the peak obtainable on-axis intensity can be calculated. As the clipping ratio decreases and more and more of the wings of the incident Gaussian beam are blocked by the aperture, mirror, lens edges, etc., diffraction effects on the beam's propagation and focusability become non-negligible and limit the theoretical peak obtainable intensity of the beam. Figure 5 is a plot of peak obtainable intensities using either Eq. 34 or Eq. 38, normalized to the peak obtainable intensity for an unperturbed focused TEM_{00} Gaussian beam. The parameters chosen for calculation of Fig. 5 are a wavelength of $\lambda = 780$ nm, a minimum beam waist of $\omega_o = 10.1$ μm and an aperture to focal plane distance of $z_G = 20\, z_R = 8.2$ mm. These particular parameters were chosen as they match experimental parameters measured in the laboratory. Significant deviations occur between the full analytical expression, Eq. 34, and the simpler approximated expression, Eq. 38, for clipping ratios $\lesssim 1$.

The primary reason for the deviation is the fact that the values plotted for the 'full' analytical solution in Fig. 5 are the peak intensities obtained for *any* on-axis position. The values calculated using the 'approximated' expression are the peak intensities in the focal plane (fixed $z = z_G$ value). For purely Gaussian beams (large γ values), the peak on-axis intensity always occurs at the focal plane. For purely diffracted beams, ($0 \lesssim \gamma \ll 1$), the peak on-axis intensity value occurs for $z = r_c^2/\lambda$. As the aperture gets smaller, the diffraction peak intensity moves closer

#121792 - $15.00 USD Received 21 Dec 2009; revised 7 Feb 2010; accepted 9 Feb 2010; published 16 Feb 2010

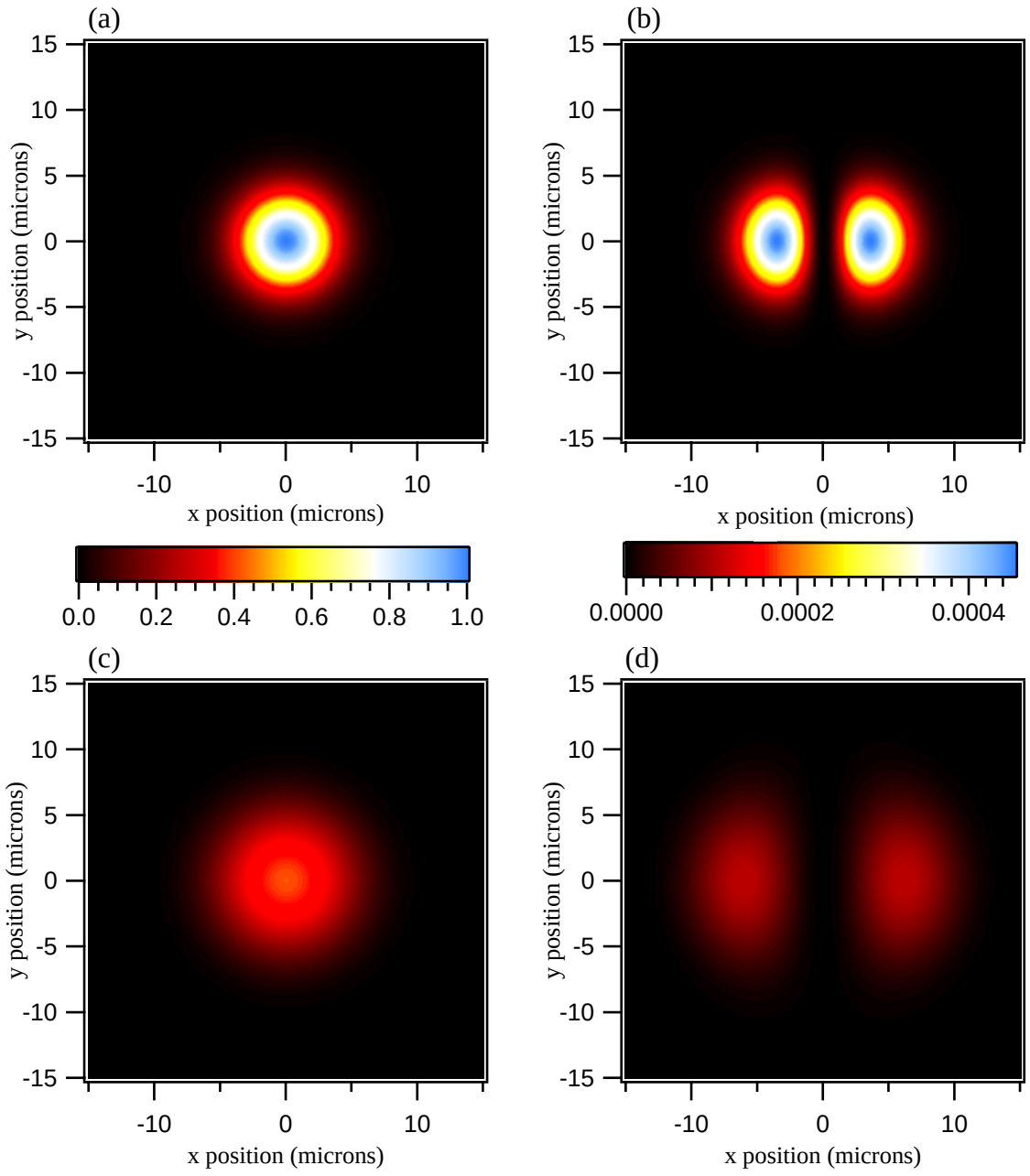

Fig. 3. Beam intensity profiles in the focal plane, $z = z_G$, for (a) $|E_x|^2$ with $\gamma = 3$, (b) $|E_z|^2$ with $\gamma = 3$, (c) $|E_x|^2$ with $\gamma = 1$, and (d) $|E_z|^2$ with $\gamma = 1$. The color scalings of (a) and (c) are both normalized to the peak intensity of (a), while the color scalings of (b) and (d) are both normalized to the peak intensity of (b). All figures are for $\omega_o = 5\mu$m, $z_G = 10$ mm and $\lambda = 780$ nm.

#121792 - $15.00 USD Received 21 Dec 2009; revised 7 Feb 2010; accepted 9 Feb 2010; published 16 Feb 2010

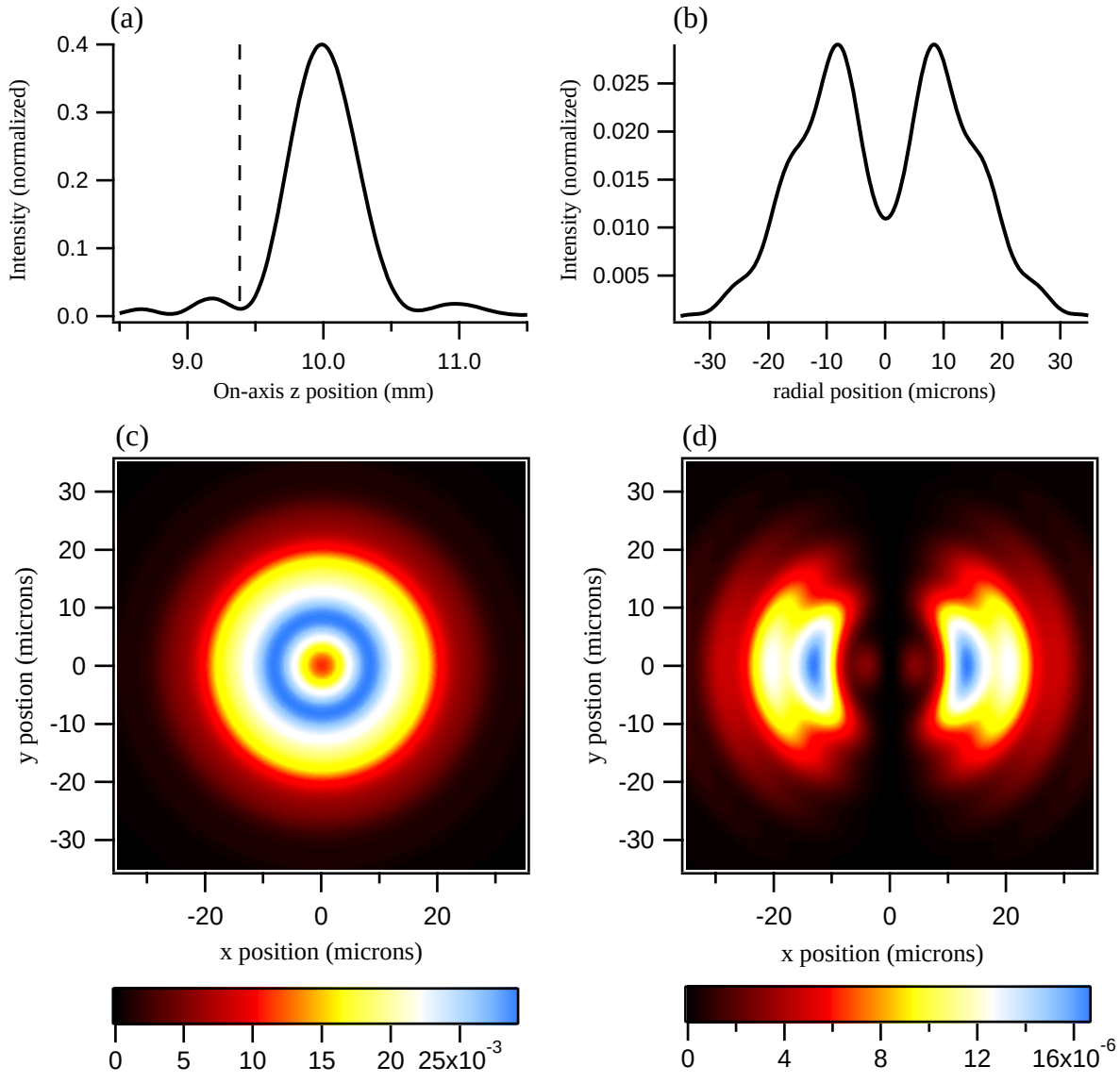

Fig. 4. (a) On-axis intensity, (b) radial intensity for an on-axis position of the on-axis minimum at $z = 9.385$ mm, (c) beam profile of $|E_x|^2$ for $z = 9.385$ mm, and (d) the beam profile of $|E_z|^2$ for $z = 9.385$ mm. All figures are for $\gamma = 1$, $\omega_o = 5\mu$m, $z_G = 10$ mm, and $\lambda = 780$ nm.

#121792 - $15.00 USD Received 21 Dec 2009; revised 7 Feb 2010; accepted 9 Feb 2010; published 16 Feb 2010

and closer to the aperture. This behavior is observed in Fig. 6 which is a collection of on-axis calculations using Eq. 34 for various clipping ratios. For example, the difference between the full and approximated values for $\gamma = 1$ in Fig. 5 is due to the shift of the peak intensity from the unperturbed focal plane towards the aperture as observed in the green line of Fig. 6. In addition to the shift of the peak intensity towards the aperture for smaller clipping ratios, another important effect of the diffraction on the focal behavior of clipped beams is the observed asymmetry of the on-axis intensity. As diffraction effects play a more significant role for smaller values of γ, the on-axis behavior of the intensity deviates from the symmetrical Lorentzian distributions for pure TEM_{00} Gaussian beams, and begins to resemble the oscillatory and asymmetrical behavior of diffracted plane waves [17].

The laser system used in the experimental verification of this manuscript is a New Focus TLB-7000 StableWave Laser controlled by the TLB-6000 Vortex Laser Controller. The diode laser cavity is tuned for an output of 780.24 nm. As is common with most diode-based laser cavities the output of the system is not that of a pure TEM_{00} Gaussian beam. The output of the laser head contains some higher-mode Hermite-Gaussian contributions and is slightly elliptical. To remove the higher-order Hermite-Gaussian modes, a spatial filter was built and optimized. The output of the spatial filter is near TEM_{00} but still contains some ellipticity. In order to remove the ellipticity of the beam profile and to overall improve the beam to establish a baseline circular TEM_{00} mode, the beam is coupled into a coiled single-mode fiber optic cable. The output of the single-mode fiber is collimated using an aspheric lens, which yields a final beam propagation of that of a near-perfect TEM_{00} Gaussian beam with an average ellipticity of $\cong$ 0.99, and an unperturbed beam propagation factor of $M^2 = 1.0$. All beam propagation, width and intensity measurements presented here are obtained using a ThorLabs BP104-IR Optical Beam Profiler with a BP1M2-150 M^2 beam quality extension set. Beam widths and profiles obtained

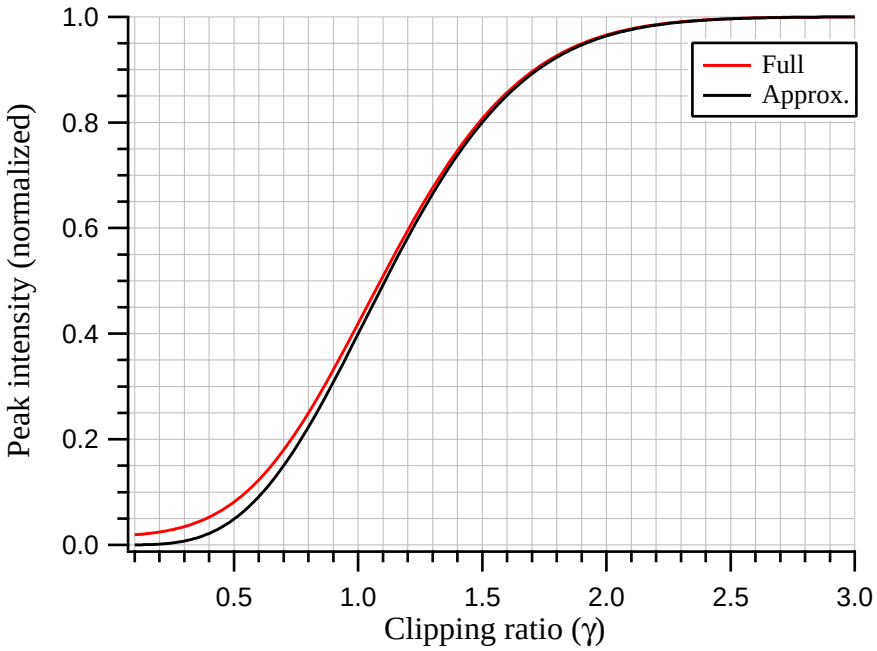

Fig. 5. Calculated peak intensities versus the clipping ratio using the full analytical expression, Eq. 34, and the simpler approximated expression, Eq. 38

.

#121792 - $15.00 USD Received 21 Dec 2009; revised 7 Feb 2010; accepted 9 Feb 2010; published 16 Feb 2010

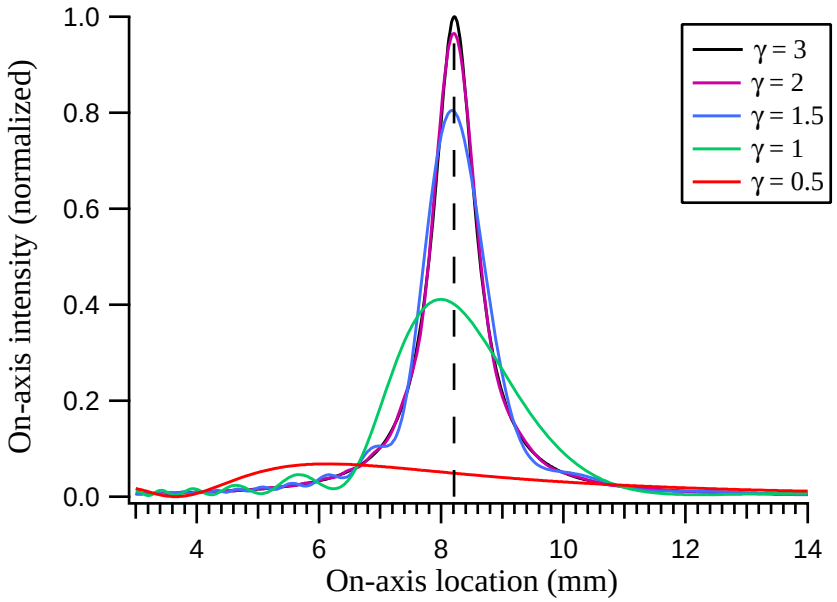

Fig. 6. Calculated on-axis intensities using the analytical model for clipping ratios of 3, 2, 1.5, 1, and 0.5. The dashed vertical line corresponds to the unperturbed focal plane.

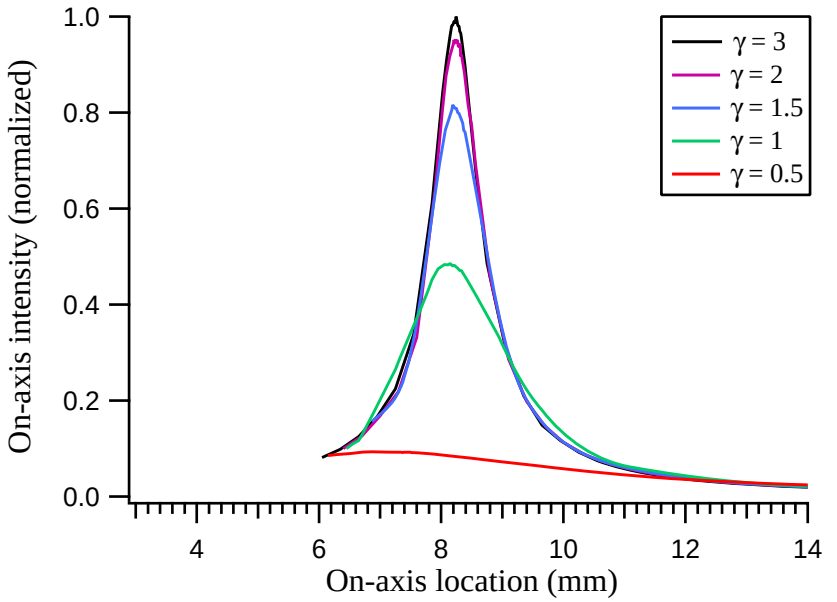

Fig. 7. Experimentally measured on-axis intensities for clipping ratios of 3, 2, 1,5, 1, and 0.5. The abrupt cutoff $\sim$ 6 mm is due to physical limitations between the aperture mount and the face of the beam profiler. All intensities are normalized to the peak of an unperturbed beam.

#121792 - $15.00 USD Received 21 Dec 2009; revised 7 Feb 2010; accepted 9 Feb 2010; published 16 Feb 2010

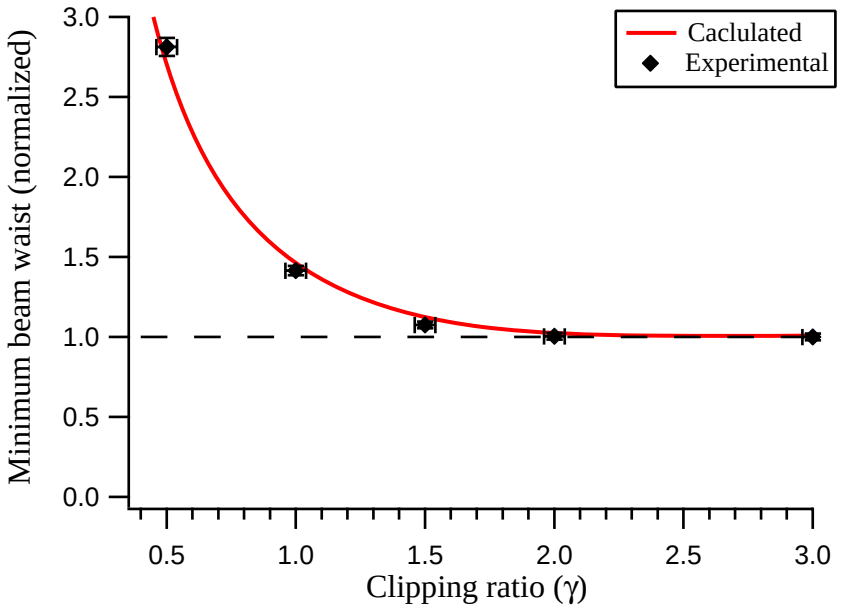

Fig. 8. Calculated and experimentally measured minimum beam e^{-2} half-widths of the intensity. Calculations were performed using the general integral solution Eq. 8.

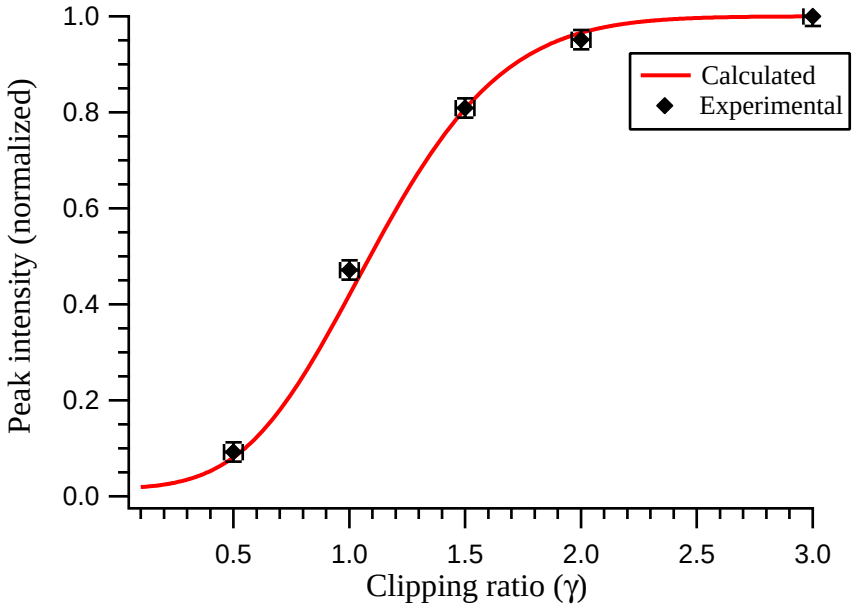

Fig. 9. Calculated and experimentally measured peak intensities. Calculations were performed using the full analytical expression, Eq. 34, and experimentally measured peak intensities are normalized to the peak intensity of an unperturbed beam.

#121792 - $15.00 USD Received 21 Dec 2009; revised 7 Feb 2010; accepted 9 Feb 2010; published 16 Feb 2010

using the beam profiler were also verified using scanning slit and pinhole techniques. Using a 75-mm focal length lens, a minimum beam waist of $\omega_o = 10.1\ \mu$m is obtained with a Rayleigh range of $z_R = 411\ \mu$m. The location of the aperture plane was chosen to be $z_G = 20z_R = 8.2$ mm.

Figure 7 is a collection of experimentally measured on-axis intensity distributions for the same clipping ratios used in the calculations for Fig. 6. The measured unperturbed beam width in the location of the aperture is $\omega_a = 201\ \mu$m. Commercially available precision pinholes from Melles Griot are used to provide various clipping ratios. The abrupt cutoff observed in Fig. 7 around 6 mm is a result of the physical limitations of the minimum distance between the pinhole foil and the scanning slits of the beam profiler due to the pinhole mount and holder and the front housing of the beam profiler. All recorded intensity values are normalized to the peak intensity of the unperturbed focused beam. For clipping ratios of $\gamma \lesssim 1$, the shifting of the peak intensity towards the aperture plane as well as the asymmetrical on-axis predicted intensity distributions are observed.

Figure 8 is a comparison of theoretically predicted and experimentally measured minimum beam widths of clipped focused-Gaussian beams as a function of the clipping ratio. The width is calculated/measured for the minimum beam width at any axial location beyond the aperture. For clipping ratios > 1 the minimum occurs at the unperturbed focal plane. For clipping ratios $\lesssim 1$ the minimum beam waist moves closer to the aperture. Both the calculated and experimentally measured width values are normalized to the width of an unperturbed focused-Gaussian beam, or ω_o. The theoretically predicted normalized e^{-2} widths of the intensity for clipping ratios of 2, 1.5, 1, and 0.5 are 1.02, 1.12, 1.46, and 2.7, respectively. Similarly, Fig. 9 is a comparison of theoretically predicted peak intensity values compared to experimentally measured peak intensities. Theoretical calculations are performed using the full analytical expression, Eq. 34. The peak intensities graphed are the maximum intensities beyond the aperture plane, and normalized to the peak obtainable intensity for an unperturbed beam. For lower clipping ratio values where the full, Eq. 34, and approximated, Eq. 38, expressions deviate from one another, the experimentally measured peak intensities best match that of the full analytical on-axis model. The axial locations of both the calculated and measured peak intensities coincide with the axial location of the minimum beam waist. A closer inspection of the beam width and peak intensity values for a clipping ratio of $\gamma = 1$ demonstrates the strong effects of diffraction on the focusability of clipped beams. For a clipping ratio of 1 only 15.7 % of the energy of the beam is being blocked by the aperture, yet the beam width has increased by 46 % and the peak obtainable intensity has decreased by 58 %. As Figs. 8 and 9 illustrate, good agreement is observed between theoretically predicted values using the model presented here, and experimentally measured values in a laboratory setting.

5. Conclusion

Two vector diffraction theories have been applied to the case of a focused-Gaussian beam which is partially blocked by a spatially limiting aperture. Using the established GHVDT, calculations were performed to investigate the dependence of beam width on axial position for a variety of clipping ratios. Calculated results illustrate that traditional M^2 beam propagation models are not appropriate for clipped focused-Gaussian beams. In this manuscript, Luneberg's vector diffraction theory is applied to clipped focused-Gaussian beams and general integral solutions for the vector electric field components have been presented. Using Fresnel approximations, simpler integral results have been derived for points of interest beyond the aperture plane. For on-axis positions of interest, an analytical model for the electric field and intensity distributions as a function of the clipping ratio is presented. Calculations using the vector diffraction model match those using the full GHVDT for points of interest within the region of validity of the Fresnel approximations. The effects of clipping on the propagation of focused-Gaussian present

#121792 - $15.00 USD Received 21 Dec 2009; revised 7 Feb 2010; accepted 9 Feb 2010; published 16 Feb 2010

themselves as: (1) asymmetrical behavior of beam width and on-axis intensity distributions for axial distances before and after the focal plane, (2) an increase in the minimum beam width, (3) a decrease in the maximum obtainable intensity, (4) and a shift of the peak intensity location towards the aperture plane. Experimental measurements for clipped focused-Gaussian beams have been conducted and quantitatively agree with calculated predictions. All of the behaviors predicted using the propagation model presented in this manuscript were experimentally observed for clipped focused-Gaussian beams.

#121792 - $15.00 USD Received 21 Dec 2009; revised 7 Feb 2010; accepted 9 Feb 2010; published 16 Feb 2010